Application of the L-Wigner Distribution to the Diagnosis of Local Defects of Gear Tooth

Sang-Kwon Lee*

(*Received April 30, 1998*)

The detection of impulsive signals causing the fracture of gears is a significant task for the analysis of the characteristics of a damaged gear. However, this impulsive signal is hidden by background noise such as meshing frequencies and broadband noise. Recently, conventional time frequency methods have been used. In the case of a signal with a low SNR, these methods are not sufficient for the detection of impulsive signals ; hence, the L-Wigner distribution with an S-method kernel is used and applied to the diagnosis of local defects of a tooth in a gear.

Key Words : Gear, Local Defect, Wigner Distribution, Diagnosis

1. Introduction

The vibration signal measured on rotating machinery is useful for system identification (Han, et al., 1998) . Especially, several studies on detection and diagnosis for gear fault have been made the using vibration signal analysis (Randall, etal., 1982 and Lee, etal., 1997a). In general it is known that the vibration signal measured on the gear box consists of the meshing frequency, its harmonic orders, side band, ghost components and broadband noise (McFadden, et al., 1987). When the tooth has been damaged by the spall, side band components of meshing frequencies increases and have been used as an indicator for the early detection of tooth damage (Wang, et al., 1996). These increased side band components are formed by amplitude and frequency modulated transient vibration signal (*i. e.*, impulsive signals are produced in the vibration signal), and are hidden by background noise such as the gear meshing frequency, its harmonics and broadband noise. The time average method and the two stage Adaptive Line Enhancer (ALE) have been used as tools to reduce the background noise and then enhance the SNR (Signal to Noise Ratio) (Lee, 1997b). However, when fracture of a tooth occurs, there are some cases where the amplitude of the impulsive signal in the vibration signal is larger than the amplitude of the meshing vibration. In this case, the amplitude of the impulsive signal is the convolution between the impact force and the system transfer function. The amplitude of the impact force is a function of velocity which in turn is proportional to the circumferential clearance of tooth contacts and the actual width of the tooth. The system transfer functions of a gear depend on the pattern of damage. Therefore, the correct detection and analysis of the impulsive signal make the pattern analysis of the gear damage easy. However, it sometimes is difficult to detect the impulsive signal because the impact force excites a lot of the frequency band and produces the complex vibration signal. Recently, in order to detect the impulsive signal, the use of the time-frequency and time scale methods increases. However, in some cases, it is difficult for the conventional time frequency methods to detect the impulsive signal with a lower SNR (Signal to Noise ratio). In this case, the higher order time frequency method is a useful tool ; In particular, the L-Wigner distribution is useful for detection of an impulsive signal with a wide band frequency.

In this paper, the conventional time frequency methods and the L-Wigner distribution (Stan-

* NVH /Chassis Part, Technology Centre, Samsung Motor Company

kovič, 1994) were applied to the data set signals measured on the gear box with local defection of a tooth. The test was carried out using 32 blocks. The data length of each block is one revolution of pinion. In order to analysis the characteristics of the damaged gear, the probability density function (PDF) was obtained by using hypothesis testing. According to these results, the PDF by using the L-Wigner distribution a was more suitable detector for the characteristics analysis of the damaged gear than the conventional time frequency distribution.

2. The L-Wigner distribution

A dual form of WHOMS (Wigner Higher Order Moment Spectra) is introduced by Stanković, and it called the multitime WHOMS. In the multitime WHOMS, if we choose the principal sliced lag axis, we can obtain the L-Wigner distribution. The L-Wigner distribution has been developed for a nonlinear FM (Frequency Modulation) signal. However, for a multi-component signal, the L-Wigner distribution has cross-terms similar to the Wigner distribution. In some cases, there are non-oscillating cross terms which are not smoothed by the conventional kernel function (Cohen, 1995). In order to smooth them the modified L-distribution (Staszewski, et al., 1997) has been developed using "S methods".

2.1 Definition of the L-Wigner distribution

The multi-time WHOMS is defined by

$$W_{n+1}(f, t_1, \cdots, t_n) = \int_{\xi} s\left(\sum_{i=1}^{n} t_i + \frac{1}{n+1}\tau\right) \prod_{i=1}^{n} s^*\left(t_i - \frac{1}{n+1}\tau\right) e^{-j2\pi f\tau} d\tau \quad (1)$$

where n is the order. When the order n is one, the multi-time WHOMS is the Wigner-Ville distribution. The multi-time WHOMS for the multi-component signal suffer from a number of cross terms (Lee, 1998). For a two component signal, the number of cross terms is 2^{n+1}. In order to overcome this problem, if we take the principal plane $(t_1 = -t_2 = t_3 = -t_4, \cdots, t_n)$ in the multi-time WHOMS, eq. (1) is written as follow:

$$W_L(t, f) = \int_{\tau} s^{L*}\left(t - \frac{\tau}{2L}\right) s^{L}\left(t + \frac{\tau}{2L}\right) e^{-j2\pi\tau} d\tau \quad (2)$$

Equation (2) is called the L-Wigner distribution (LWD). When $L=1$, the LWD is the Wigner-Ville distribution (WVD). The number of cross terms of the LWD for a two-component signal is oscillating in mid point between two components like WVD's. However, the number of cross terms of the LWD for s signal with components at the same time, but at different frequency, increase dramatically as L increases. In this case, the non-oscillating cross term also appears between two

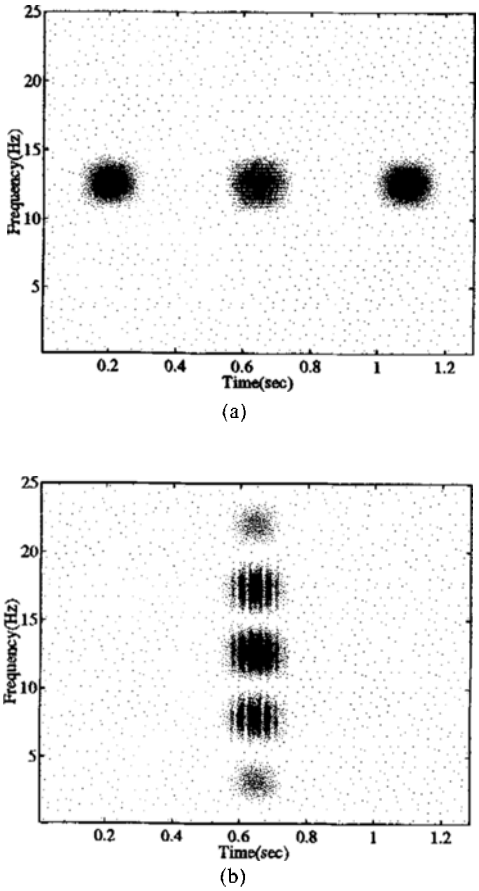

Fig. 1 The L-Wigner distribution (L=2) for the two components signal (a) components centred at 0.2 s with 3Hz and at 1.08 with 22Hz (b) components centred at 0.64s with 3Hz and 22Hz

components. This non-oscillating cross term cannot be smoothed by conventional methods.

These observations are verified via a pair of simulations, the results of which are shown in Fig. 1. In both cases the LWD is computed for a 128 point time series at an assumed sampling rate of 100 Hz and in both cases the signal consists of two complex exponential amplitudes modulated by a Gaussian envelope. The first example contains two components occurring at different times, 0.2 and 1.08 s, but at the same frequency, 12.5 Hz. The LWD for this signal is shown in Fig. 1(a). This plot uses a linear grey scale on which dark levels depict high values and in which negative values have been set to zero. The middle component is the cross-term, whose oscillatory nature can be seen. Such a plot is visually similar to that one would anticipate from a WVD. In the second case, the signal components occur at the same time, centred on $t=0.64$, but at different centre frequencies, specifically 3 and 22Hz. The LWD of this signal is shown in Fig. 1(b). In this case there are three sets of cross-terms, in contrast to a WVD which would only generate a single set of cross-terms. The LWD cross-terms appear at quarter intervals between the two components. The off-centre cross-terms at 1/4 and 3/4 of the interval are oscillatory albeit only in the time direction. However, the cross-terms appearing at the mid point contains both an oscillatory element and a non-oscillating element.

2.2 The smoothing of the L-Wigner distribution for a multi-component signal

2.2.1 Smoothing using conventional methods

For the multiple signals, Cohen's class of distributions has been developed to reduce and smooth cross terms using a variety of kernels (exponential, cone, ···, etc.). Similarly the L-class time frequency is defined as,

$$L(t, f)=\iiint_{\xi\, u\, \tau}\phi_L(\xi, \tau)\, s^{L*}(u-\frac{\tau}{2L})\, s^{L}(u+\frac{\tau}{2L})\, e^{-j2\pi(f\tau+\xi u-\xi t)}\, du d\xi d\tau \quad (3)$$

For $L=1$ this is the Cohen's class of time frequency representation. The general properties of this distribution are discussed in Ref. (Stankovič, 1996). A Fourier transformed form of eq. (3) is given by

$$L(t, f)=\iiint_{\xi\, u\, \tau}\phi_L(\xi, \tau)\, s^{L*}(Lu-\frac{\xi}{L})\, s^{L}(u+\frac{\xi}{L})\, e^{-j2\pi(f\tau+\tau u-\xi t)}\, du d\xi d\tau \quad (4)$$

The L-ambiguity function associated with L-class of distribution is given by

$$A_{Lf}(\xi, \tau)=\int_{u} s^{L*}(u-\frac{\tau}{2})\, s(u+\frac{\tau}{2})\, e^{-j2\pi\xi u}\, du \quad (5)$$

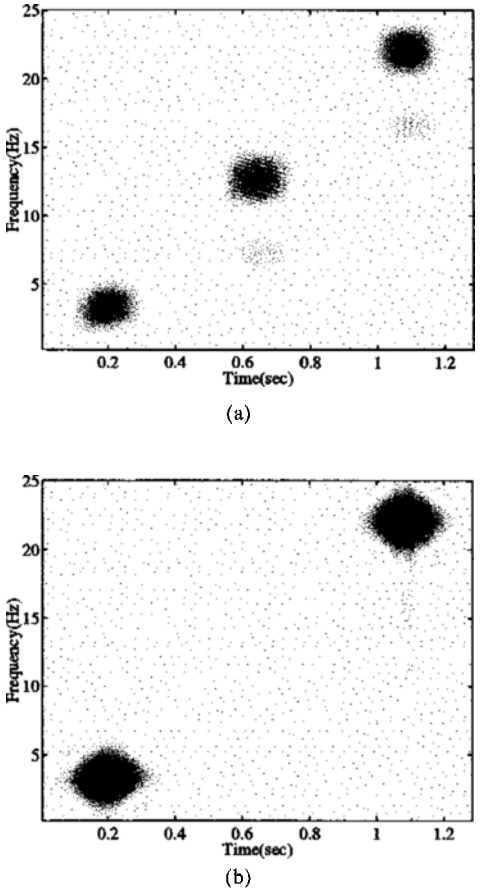

Fig. 2 Comparison of the LWD and the LWD with Choi-Williams for the two components signal centred at 0.2 s with 3Hz and at1. 08 with 22Hz (a) The LWD (b) The LWD with Choi-Williams kernel.

and the L-general ambiguity function is defined as

$$A_{Lg}(\xi, \tau) = A_{Lf}(\xi, \tau) \cdot \phi_L(\xi, \tau) \qquad (6)$$

The kernel $\phi_L(\xi, \tau)$ is the same as the kernel of the Cohen's class of time frequency representation.

The effectiveness of smoothing the LWD using an exponential kernel is demonstrated via a few simple simulations. Figure 2 depicts the LWD calculated for a signal containing two components in a 128 point time series, sampled at 100Hz. Each component is a Gaussian modulated complex sinusoid ; the first component is centred in the time frequency plane at 0.2 s and 3 Hz, the second component is centred about 1.08s and 22 Hz. Figure 2(a) shows the unsmoothed LWD (L =2) in which the interference term is clearly evident as an oscillatory component midway between the two auto-terms. Figure 2(b) shows the result of applying an exponential kernel. In this case the interference term has been removed at the cost of some distortion to the auto-terms.

Figure 3 shows the results of applying the exponential kernel to the data depicted in Fig. 1. The results of this simulation are less satisfying since the exponential kernel is poorly suited to removing cross-terms between vertically and horizontally displaced components, especially in fig. 3 (b), since it is impossible to smooth non-oscillating cross-terms by using the exponential kernel function.

In summary, the LWD can generate cross-terms which conventional smoothing fails to attenuate effectively.

2.2.2 Smoothing of non-oscillating cross -terms in the LWD

In order to effectively smooth the non-oscillating cross-terms in the LWD, consider the Wigner -Ville distribution,

$$W(t, f) = \int_{\tau} s\left(t+\frac{1}{2}\tau\right) s^* \left(t-\frac{1}{2}\tau\right) e^{-j2f\tau t} d\tau \qquad (7)$$

The pseudo Wigner distribution (PWD) can be written using the time domain windowing function $h(\tau/2)$ as follows:

$$W_{pw}(t, f) = \int_{\tau} h\left(\frac{\tau}{2}\right) h^*\left(-\frac{\tau}{2}\right) s\left(t+\frac{1}{2}\tau\right) s^* \left(t-\frac{1}{2}\tau\right) e^{-j2f\tau} d\tau = \frac{1}{2}\int_{\tau'} h(\tau')\, h^*(-\tau')\, s(t+\tau')\, s^*(t-\tau')\, e^{-j2\pi(2f)\tau'} d\tau' \qquad (8)$$

where $\tau' = \tau/2$. Using convolution, equation (8) may be written as follows:

$$W_{pw}(t, f) = S_H(t, 2f) \times S_H^*(t, 2f) \qquad (9)$$

where $S_H(f, t)$ is the STSF. Therefore, the PWD can be written as,

$$W_{pw}(t, f) = S_H(t, 2f) \underset{f}{*} S_H^*(t, 2f)$$

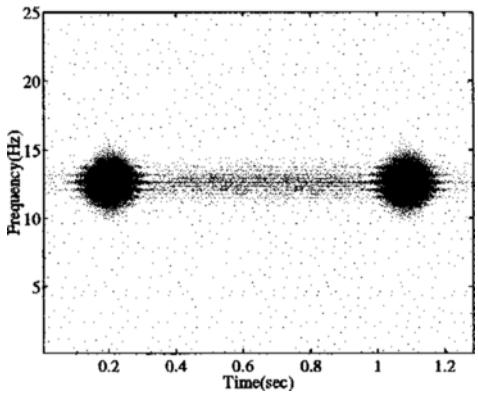

(a)

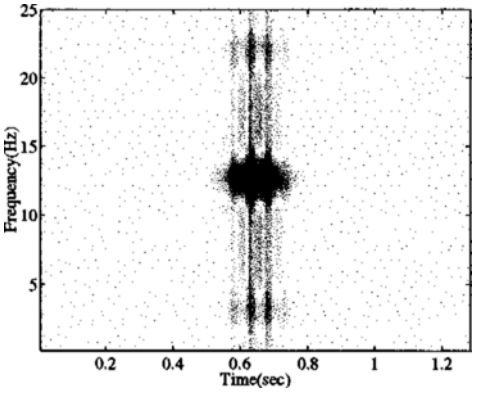

(b)

Fig. 3 Comparison of the LWD and the LWD with Choi-Williams for the two components signal ; (a) components centred at 0.2 s with 3Hz and at 1.08 with 22Hz (b) components centred at 0.64 s with 3Hz and 22Hz

$$=\int_{-\infty}^{\infty} S_H(t, f+\xi)\, S_H^*(t, f-\xi)\, d\xi \tag{10}$$

In order to emphasise the auto-terms of the PWD for a multi-component signal, a window function $\Gamma(\xi)$ can be incorporated into eq. (10) and the smoothed pseudo Wigner distribution (SPWD) can be developed as follows:

$$W_{L=1,spw}(t, f) = \int_{-\infty}^{\infty} \Gamma(\xi)\, S_H^*(t, f+\xi)\, S_H^* (t, f-\xi)\, d\xi \tag{11}$$

Therefore, using the ambiguity (O'Neill, 1995) plane (ξ, τ), the kernel function for this window function $\Gamma(\xi)$ can be developed as follows:

$$\Phi(\tau, \xi) = \Gamma(\xi) \underset{\xi}{*} A_{g,sp}(\xi, \tau) \tag{12}$$

where $A_{g,sp}(\xi, \tau)$ is the general ambiguity function associated with the spectrogram of signal $s(t)$ (Classen, 1980). We refer to this kernel function as "the S-method". In Eq. (11), when $\Gamma(\xi) = 1$, the SPWD becomes the WVD and when $\Gamma(\xi) = \delta(\xi)$ the SPWD becomes the spectrogram. Therefore, in order to smooth the cross-terms of the WVD, the duration B_Γ for $\Gamma(\xi)$ needs to be selected in accordance with,

$$B_H < B_\Gamma < \min_{i,j} \frac{f_i - f_j}{2} - B_H \tag{13}$$

where the f_i and f_j are the instantaneous frequencies of the signal components and B_H is the bandwidth of $H(f)$.

The SPWD is obtained by convolving two signals $S_H(t, 2f)$ and $S_H^*(t, 2f)$ with respect to frequency and using the S-method for smoothing the cross-terms in Eq. (11). Similarly, a smoothed version of the LWD (L=2) can also be obtained by the convolution of two SPWD $W_{L=1,spw}(t, 2f)$ and $W_{L=1}{}^*{}_{,spw}(t, 2f)$ with respect to frequency as follows:

$$W_{L=2,spw}(t, f) = \frac{1}{2}\int_{\tau} \Gamma(\xi) \cdot W_{L=1,spw} (t, f+\xi) \cdot W_{L=1,spw}(t, f-\xi)\, d\xi \tag{14}$$

Therefore, a general form of the smoothed version of the LWD can be obtained as follows:

$$W_{L+1,spw}(t, f) = \frac{1}{2}\int_{\xi} \Gamma(\xi) \cdot W_{L,spw}(t, f+\xi) \cdot W_{L,spw}(t, f-\xi)\, d\xi,\ L=1,2,3, \cdots \tag{15}$$

where $W_{L,spw}(t, f)$ is the smoothed pseudo Wigner distribution $(L=1)$ or the smoothed LWD $(L=2, 3, \cdots)$.

The effectiveness of smoothing the sliced WHOMS using the γ-method kernel and the LWD using the S-method kernel is again demonstrated via simple simulations. Figure 4(a) depicts the LWD (L=2) calculated with the same data set as used to compute Fig.(a) using the S-method and Fig. 4(b) depicts the LWD ($L=2$) calculated with the same data set as used to compute Fig. 1(b) using the S-method. In this

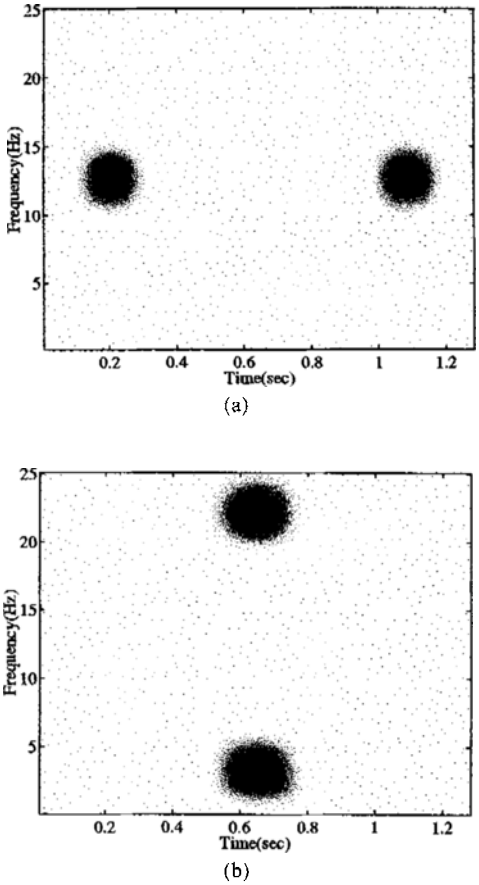

Fig. 4 (a) The SWT with γ-method kernel for the two components signal centred at 0.02 s with 3Hz and at 0.18 s with 22Hz (b) The LWD ($L=2$) with S-method kernel for the two components signal centred at 0.64 s with 3Hz and 22Hz

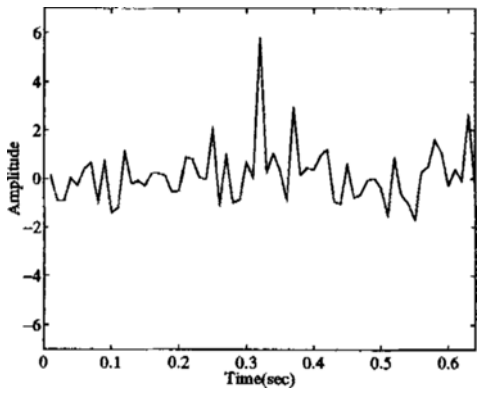

(a)

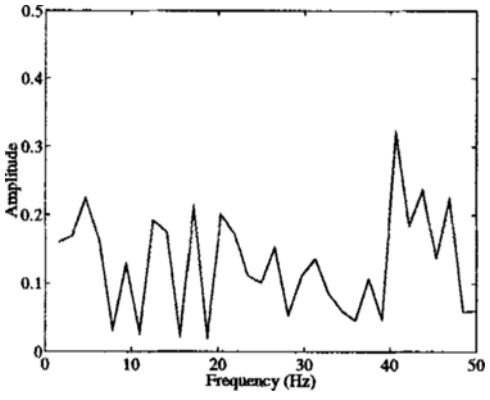

(b)

Fig. 5 A Gaussian pulse and an impulse in noise (a) Single impulse corrupted by broadband noise, (b) FFT of signal (a)

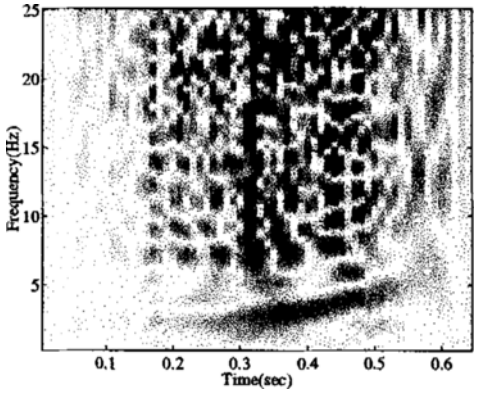

(a)

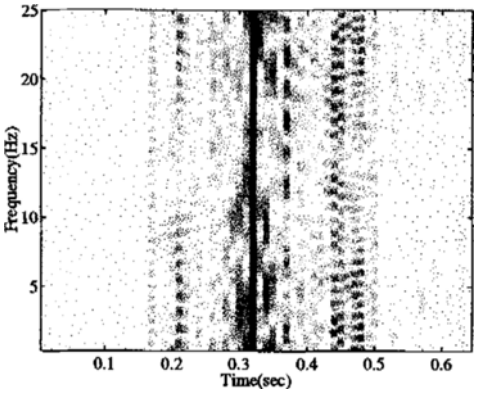

(b)

Fig. 6 Comparison of the WVD and LWD (L=2) for the impulsive signal embedded in broadband noise ; (a) The WVD (b) The LWD (L=2)

case, the sampling frequency is 100Hz, the number of samples is 512 for the f_S, $f_i - f_j = 19$Hz and $t_i - t_j = 0.88$ s. 2Hz is used as the width of the window for $\Gamma(\xi)$ and 0.64 s is the duration of the sliding window $h(\tau)$. According to these results, the non-oscillating cross-terms can be eliminated, as shown in Fig. 4(b). Therefore, in order to smooth cross-terms of the LWD, the S-method is more effective than the conventional approach adopted by Cohen's class of time frequency representations.

Finally, one of the interesting properties in the LWD is its superior detection performance of impulse embedded in the broadband noise to the WVD. In order to examine, thus consider a data set containing one component in a 128 point time series, sampled at 100 Hz. The signal component is impulsive at 0.32 s, as shown in Fig. 5(a).

The WVD and the LWD for this data set are shown in Fig. 6(a) and (b), respectively. The WVD fails to give clear information about the impulse. However, the LWD ($L=2$) for this data set does give clear information about the impulsive signal component. According to the definition of the LWD form, Eq. (2), the squaring operation in the time domain, serves to accentuate the peak. From this intuitive point of view, we can explain why the signal component is more visible in the LWD (Fig. 6(a)) than in the WVD (Fig. 6(b)).

3. Vibration Data Measured on a Gear Box

Figure 7 shows a defected tooth of a gear box which consists of 30 tooth pinions and 45 tooth wheels. This data was also used in reference (Reynolds, 1995). Fig. 7(a) shows teeth of pinion gear with partial tooth loss over 40% facewidth / 20% facewidth(at root), due to a root to root fracture : defect A. Figure 7(b) shows a similar situation but due to a face to root fracture : defect B.

Fig. 8(a) and (b) show the time history of a vibration signal measured on the gear box associated with Fig. 7(a) and (b), respectively. The sampling frequency is 8773Hz and 512 sample per cycle. In case of defect B, the impact caused by tooth fracture is clear whilst in the case of defect A, the impact is not very clear. In defect B, the impulsive vibration signal is larger than the background vibration such as meshing frequency, its harmonic components and broadband vibration. However, in defect A, the impulsive signal vibration is not much more dominant than the background vibration. These results are caused by different system transfer functions of the tooth and different impacting forces on the tooth due to different types of failure.

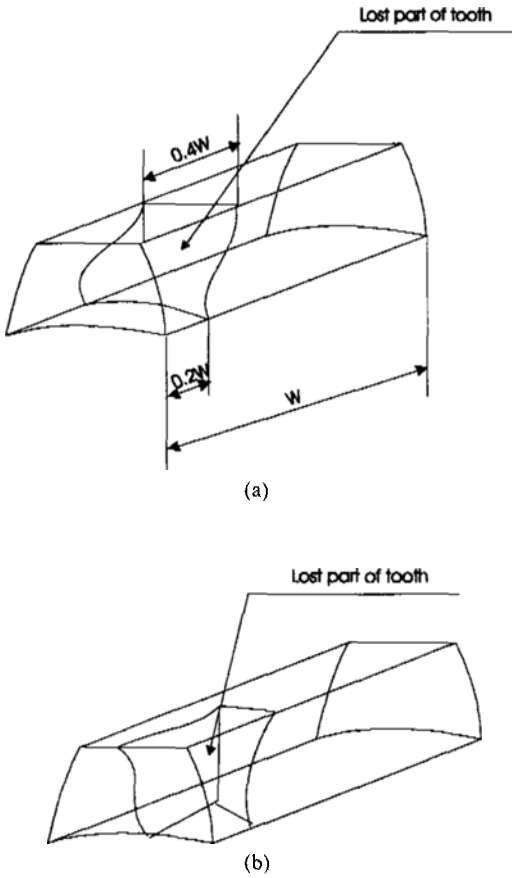

Fig. 7 The shape of local fault tooth.

4. Application of Time Frequency Methods

4.1 Application of conventional time-frequency methods

4.1.1 Application of Wigner-Ville distribution

The Wigner-Ville distribution is defined by

$$W(t, f)=\int_{-\infty}^{\infty} s(t+\frac{\tau}{2})\, s^*(t-\frac{\tau}{2})\, e^{-j2\pi f\tau} d\tau \tag{16}$$

where s(t) is the signal and τ is the time lag. The Wigner-Ville distribution has good time and frequency resolution but cross term interference as its representative properties.

Figures 9(a) and (b) show the Wigner-Ville distribution for the vibration data of defect A and defect B, respectively. The left box presents the averaged magnitude along the time axis at a certain frequency. The bottom box presents the time history for signal s(t). According to Fig. 9 (a), it is very difficult to identify the characteristics of the damaged gear because of background noise, meshing frequencies and their cross terms. In Fig. 9(b), the similar phenomenon takes places even if the impulsive signal is clear in the time domain. Therefore, the WVD is not very good time frequency method for the fault analysis of the gear failure.

In order to reduce or smooth the cross terms, the kernel function can be used. Hence, if we apply the exponential kernel function to the vibration data we can obtain the smoothed time frequency distribution called the Choi-Williams

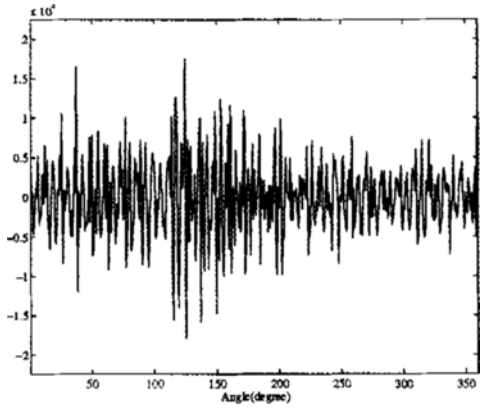

(a) Defect A ; 40% facewidth and 20% tip lost at root to root of tooth

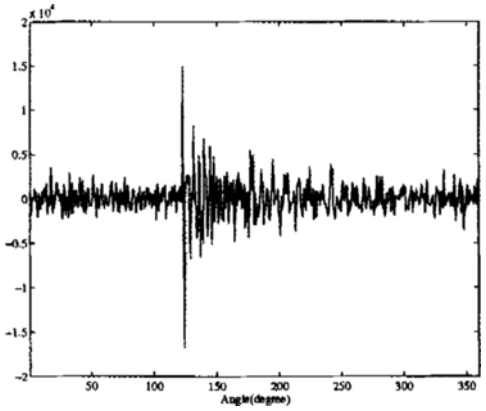

(b) Defect B ; 40% facewidth and 20% tip lost at face to root of tooth

Fig. 8 Vibration data measured on the gear box with partial lost tooth.

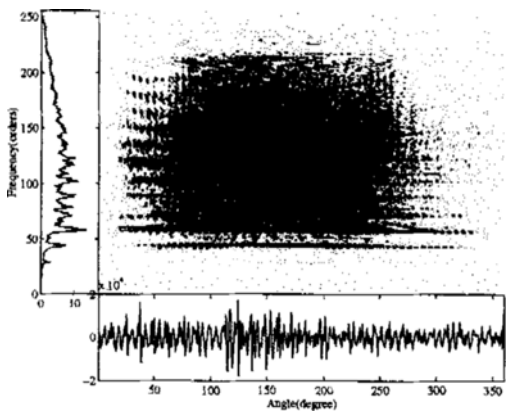

(a) Defection A ; 40% facewidth and 20% tip lost at root to root of tooth

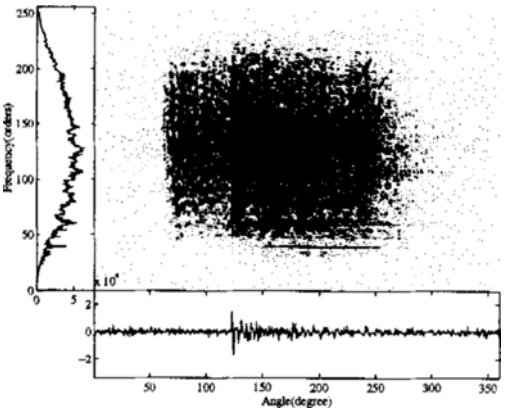

(b) Defection B ; 40% facewidth and 20% tip lost at face to root of tooth

Fig. 9 Wigner Ville distribution for the vibration data measured gear box with partial lost tooth.

distribution,

$$W_c(t,f)=\int_{\tau} e^{-j2\pi f\tau}\left[\int_{u}\frac{1}{2\tau}\sqrt{\frac{\sigma}{\pi}}e^{-j2\pi\left(fu+\frac{\sigma(u-t)^2}{4\tau^2}\right)}\cdot s\left(u+\frac{\tau}{2}\right)s^*\left(u-\frac{\tau}{2}\right)du\right]d\tau \tag{17}$$

where σ is the coefficient controlling the frequency resolution and the degree of smoothing of the cross terms.

The Choi-Williams distribution for the signal s (t) is shown in Fig. 10(a) and (b). In Fig. 10(a) we can see the meshing frequency and its harmonic frequencies clearly. The dominant impulsive signal also appeared at the 110° of shaft angle with centre frequency between 70th order and 90th order. However it is not clear due to interference by other components. However in Fig. 10(b) two dominant impulses appear at 125° and the 1st meshing frequency (30th order) appeared along to time axis clearly. Therefore the Choi-Williams distribution is sufficient for the detection of gear failure in case of defect B.

4.1.2 Application of spectrogram

The spectrogram(Cohen, 1995), a most popular and basic time frequency method, has been applied widely in the science fields for long time and is defined as

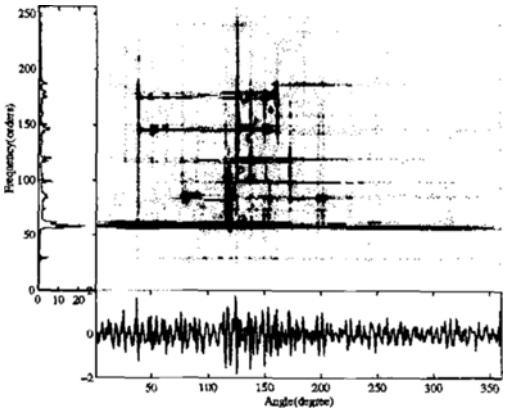

(a) Defection A : 40% facewidth and 20% tip lost at root to root of tooth

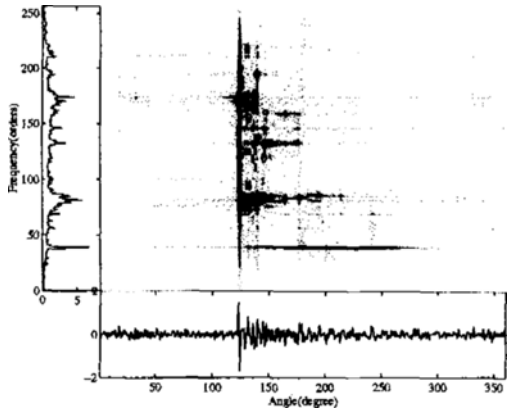

(b) Defection B : 40% facewidth and 20% tip lost at face to root of tooth

Fig. 10 Choi-Williams distribution for the vibration data measured gear box with partial lost tooth.

$$S(t, f)=\left|\int_{-\infty}^{\infty} h^*(\tau-t)\, s(\tau)\, e^{-j2\pi f\tau} d\tau\right|^2 \qquad (18)$$

where h(t) is a sliding window.

Figures 11 and 12 are the spectrogram for the vibration data measured on the gear box. Figure 11 is the result of using a large window size and Fig. 12 is the result of using a small window size. The window size must be selected carefully depending on signal. In Fig. 11(a), the 1st meshing frequency (30th order) is seen but many peaks make the decision about detection of fault of gear confuses because the dominant impulse does not appear. In Fig. 12(a) we cannot see the 1st

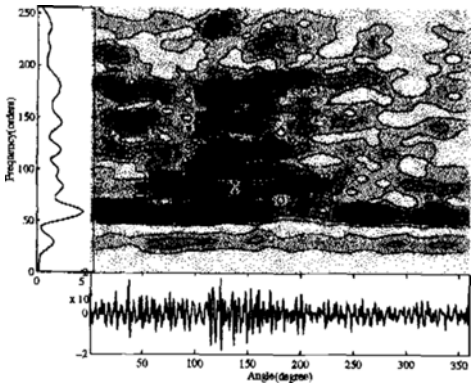

(a) Defection A : 40% facewidth and 20% tip lost at root to root of tooth

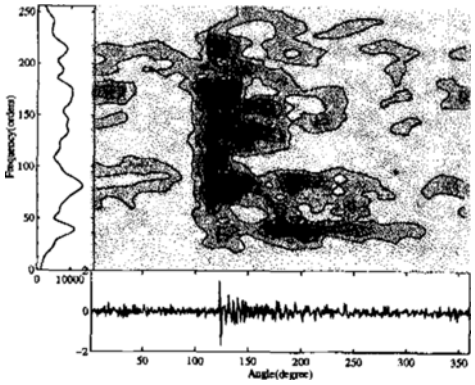

(b) Defection B : 40% facewidth and 20% tip lost at face to root of tooth

Fig. 11 Spectrogram with large hanning window size (nfft=64/512 with 50% overlap) for vibration data measured gear box with partial lost tooth.

meshing frequency due to the small window size but it is much easier to find the dominant impulse. However still many scattered peaks make the decision about the detection of faults in gear difficult. On the other hand, the spectrograms for the vibration data on gear box with defection B are shown in Fig. 11(b) and Fig. 12 (b). According to these results, in the case of defect B, the impulses are clearly shown in the plot but with poor time or frequency resolution. Thus it is not easy for the spectrogram to detect faults of a gear.

4.1.3 Wavelet analysis

Since 1980, the wavelet analysis has been rapid-

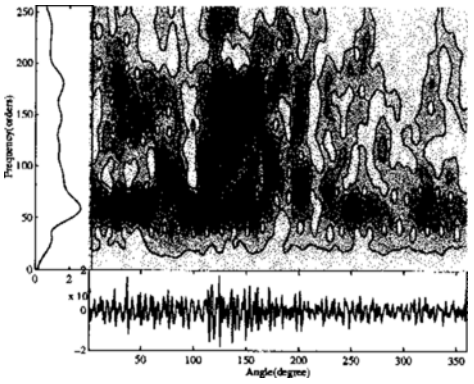

(a) Defection A : 40% facewidth and 20% tip lost at root to root of tooth

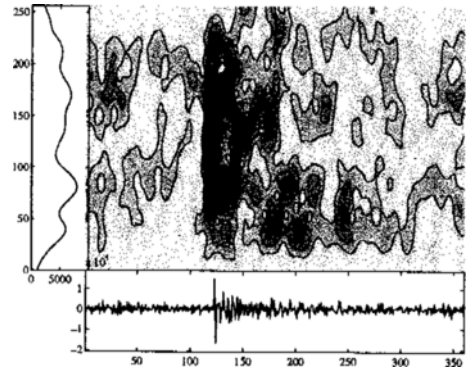

(b) Defection B : 40% facewidth and 20% tip lost at face to root of tooth

Fig. 12 Spectrogram with large hanning window size (nfft=32/512 and 30% overlap) for vibration data measured gear box with partial lost tooth.

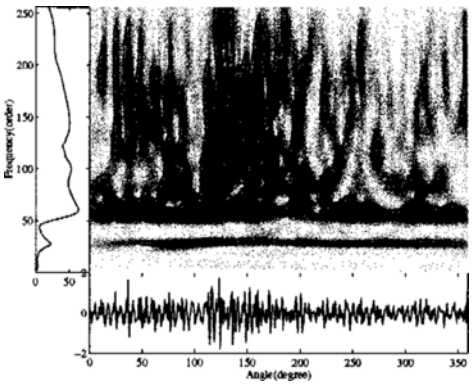

(a) Defection A : 40% facewidth and 20% tip lost at root to root of tooth

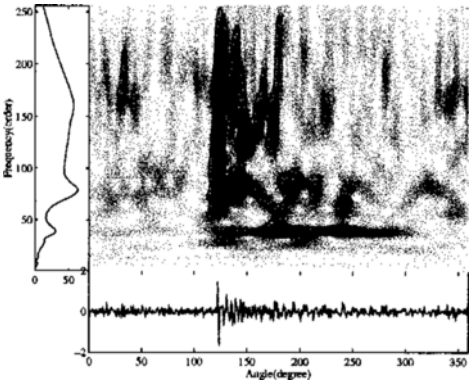

(b) Defection B : 40% facewidth and 20% tip lost at face to root of tooth

Fig. 13 Wavelet analysis using Morlet mother wavelet {(fm=1, fms=512(length of time history), La(step of frequency) =128, Lb(step of time) =128, fs=8772Hz, amin=fm/(fms/2), amax=1} for vibration data measured gear box with partial lost tooth (L =3).

ly developed and applied in many science areas (Chai, 1992). The wavelet analysis is classified as orthogonal and non-orthogonal, depending on the mother wavelet function. The representative orthogonal mother wavelet is the Daubechies (New land, 1994) wavelet function and it is useful for the imaging process. The representative non orthogonal wavelet is the Morlet wave function and is suitable for the detection and analysis of gear faults. The Morlet(kronland, 1987) wave function is defined as

$$m(t)=e^{-|t^2|}e^{i2\pi f_o|t|} \tag{19}$$

where f_o is the frequency of the wavelet. This is a form of Gaussian windowed sinusoidal function.

The decomposition wavelet coefficients is obtained by

$$W_m(a,\ b)=\frac{1}{\sqrt{a}}\int_{-\infty}^{\infty}s(t)\,m^*\left(\frac{t-b}{a}\right)dt \tag{20}$$

where a is the scale factor of frequency, and b is the scale factor of the time shift. According to eq. (20) signal s(t) can be decomposed as mother function m(t) within local time window whilst the Fourier transform signal s(t) can be decomposed as sine and cosine functions during infinite time. Thus wavelet analysis is useful for time frequency decomposition of a transient sig-

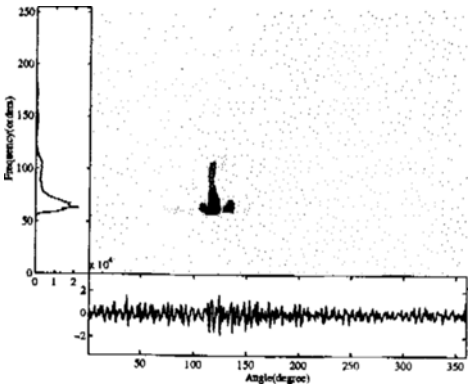

(a) Defection A : 40% facewidth and 20% tip lost at root to root of tooth

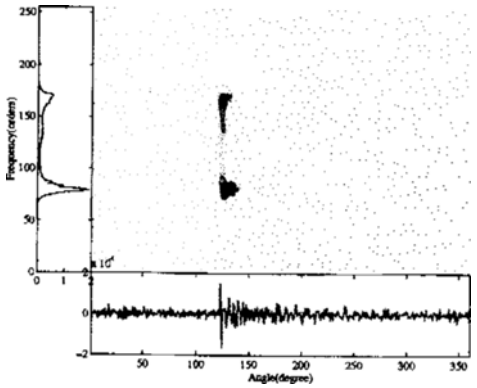

(b) Defection B : 40% facewidth and 20% tip lost at face to root of tooth

Fig. 14 L-Wigner distribution with recursively applied S-method kernel for vibration data measured gear box with partial lost tooth (L =3).

nal such as an impulsive signal. Wavelet analysis is also affected by the uncertainty principle, like the spectrogram. However, the window size can be controlled by scale factor a and b. The signal is decomposed with a narrow frequency band at lower frequencies and with a wide frequency band at high frequencies by scaling factor a as keeping the shape of the mother wavelet.

Figure 13 shows the wavelet analysis for vibration signals. The wavelet analysis for defect A gear is shown in Fig. 13(a). There are many trace about meshing frequency around 30 order (the 1 st meshing frequency) and 60orders (the 2nd meshing frequency). However, the information about the dominant impulsive signal is not clear. On the other hand, in Fig. 13(b), the information about the dominant impulsive signal is clear, like the result of the spectrogram for the same signal as shown in Fig. 12(b).

4.2 Application of the L-Wigner distribution

In case of defect A, as discussed in the previous section the conventional time frequency method is not suitable for the detection of gear faults.

Figures 14(a) and (b) show the L-Wigner distribution using the S-method for the vibration data measured on the gear box. The L-Wigner distribution for the vibration data using the gear with defect A is shown in Fig. 14(a). In this plot, we see a impulsive signal clearly at the 110° of shaft angle with centre frequency around between 70th order and 80th order. This result corresponds to the result of the Choi-Williams distribution and spectrogram but this plot emphasises the impulse signal effectively because of the squaring effect of the LWD (L=2) for the relatively large impulsive signal to meshing frequencies. For this plot, we use L=3 and S-method kernel functions. Similarly the L-Wigner distribution for the vibration data using the gear with defect B gear is shown in Fig. 14(b). In this plot the two impulses appear more clearly than those in the conventional time frequency method. The fault occurs at the 120° of shaft angle with 85th order and 170th order frequency components.

5. Discussion

The comparison between conventional time frequency methods and the L-Wigner distribution for the measured signal on the gear box has been discussed. According to the results, the L-Wigner distribution is a better solution for the detection of impulsive signals and diagnosis of gear faults. As for the more robust methods for testing performance of detection tools, the hypothesis testing can be used. If we calculate the probability density function (PDF) by using 32 cycles in measured data on a gear box, the PDF for each time frequency method is obtained as shown in Fig. 15.

For the calculation of the PDF we assume the distribution to have Gaussian distribution, but it

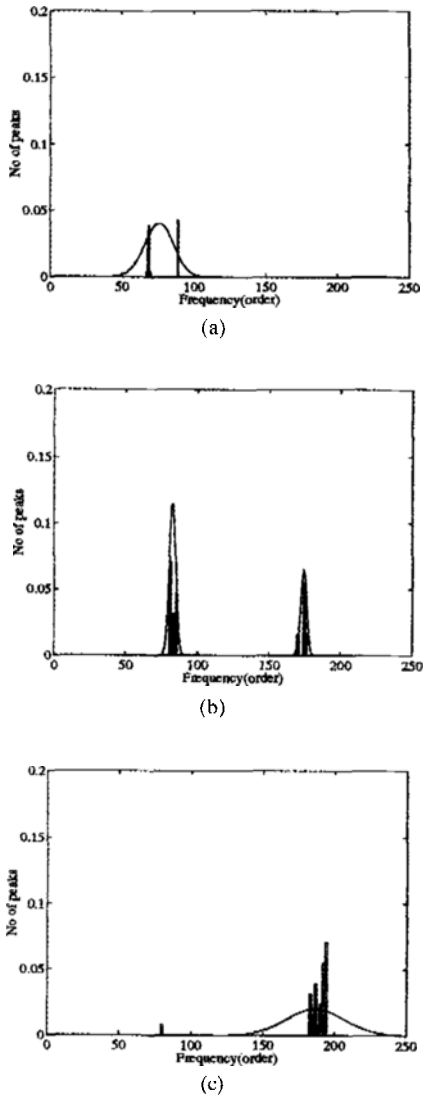

Fig. 15 Probability density function comparison for peaks by using Spectrogram (a) defection A (b) defection B (c) Normal gear.

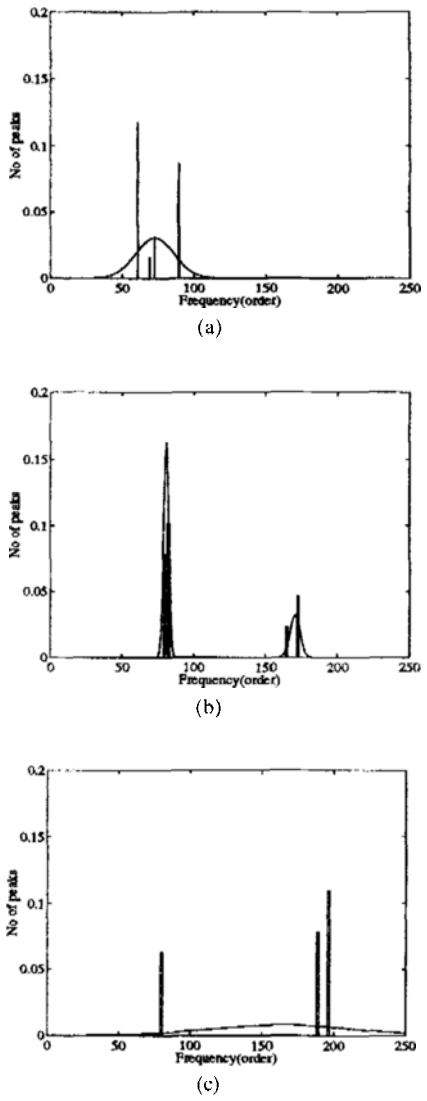

Fig. 16 Probability density function comparison for peaks by using Wavelet analysis (a) defection A (b) defection B (c) Normal gear.

is difficult to find how many Gaussian distributions are in Figs. 15, 16 and 17 via bar graphics. Therefore we use the Separability Criteria referred to in Ref. (Fukunage, 1990) (22) and the results are listed in Table. 1. If J2 is higher than 3, we can say there are two Gaussian distributions. Using this method the Gaussian distribution curve is plotted in Figs. 15, 16 and 17. According to these results, the spectrogram (Fig. 15) and wavelet analysis (Fig. 16) for defect A have the PDF with large variation. Thus, both time and frequency methods will give some confusions for decision between fault and normal gear at lower frequency bands around 60-100 order. The reason for this phenomenon is that both time frequency methods are affected by the uncertainty principle. The PDF by using the L-Wigner distribution shown in Fig. 17 is more useful for identifying the dominant faulty and distinguishing between fault and normal because the PDF curves have a narrow band of variation and are separated.

Table 1 Separability criteria (J2)

	Fault 1 (Defect A)	Fault 2 (Defect B)	Normal
Spectrogram	NaN	5.9702	NaN
Wavelt Analysis	NaN	5.6715	NaN
Modified L-Wigner	4.4296	6.0797	2.2841

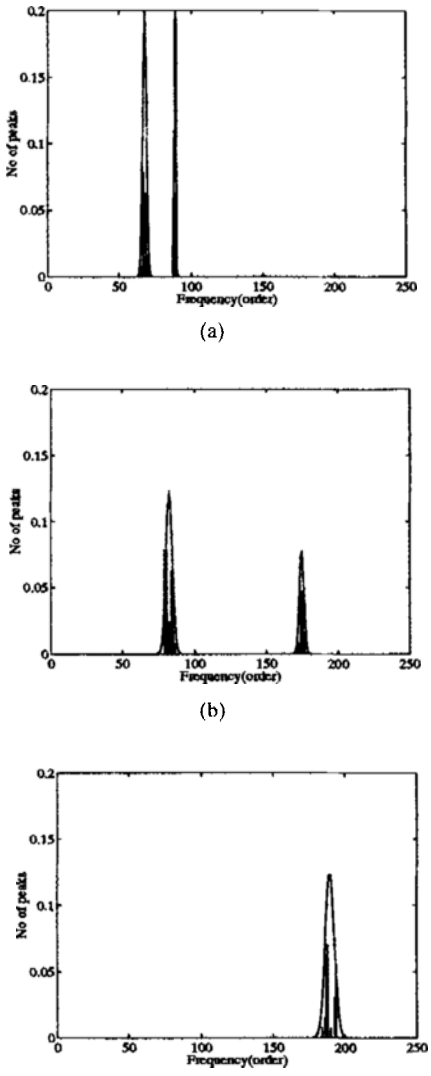

Fig. 17 Probability density function comparison for peaks by using the L-Wigner Distribution ; (a) defection A (b) defection B (c) Normal gear

6. Conclusion

For the convenient detection of local gear defect, the L-Wigner distribution is discussed and applied to a data set measured on the gear box. Compared to the conventional methods such as the spectrogram, Wigner-Ville distribution and wavelet analysis, the L-Wigner distribution has the advantage of enhancing the impulsive signal. This properties is useful tools in the diagnosis of typical gear faults like local defect. The hypothesis testing for the detection performance demonstrates that the L-Wigner distribution has better detection performance than the conventional time frequency method and is very helpful in the characteristic analysis of gear damage.

Reference

Chui, C. K, 1992, "Introduction to wavelets," Academic Press Inc.

Claasen, T. and Mecklenbrauker, W., 1980, "The Wigner distribution-A tool for time-frequency signal analysis : part Ⅰ, Ⅱ, Ⅲ," Phil. J. Res., Vol. 35, No. 3, p. 217~389.

Cohen, L., 1995, "Time-Frequency Analysis," Prentice hall.

D. E Newland, 1994, "An introduction to random vibrations, spectral and wavelet analysis," The 3rd edition.

Fukunaga, K, 1990, "Introduction to statistical Pattern Recognition," 2nd edition, Academic Press.

Han, D. C. and Choi, S. H. and Lee, Y. H. 1998, "The Nonlinear and Ball Effects of a Ball Bearing on Rotor Vibration," KSME International Journal, Vol. 12, No. 3, pp. 396~404.

Kronland-Martinet, R. and Morlet, J., 1987, "Analysis of sound through wavelet transforms," International Journal of Pattern Recognition and Artificial Intelligence, Vol. 1, pp. 273~302.

Lee, S. K and White, P. R., 1997a, "Fault Detection and Analysis in Rotating Machinery Using Higher Order Time Frequency Method" 10th International Congress and Exhibition on Conditional Monitoring and Diagnostic Engi-

neering Management, Vol. 1, pp. 313~412.

Lee, S. K. and White, P. R., 1997b, "Fault identification for rotating machinery using adaptive signal processing and time-frequency analysis" 1997 ASME Design Engineering Technical Conferences, 16th Biennial Conference on Mechanical Vibration and Noise, Symposium on Mechanical Condition Monitoring, Sacramento, California, USA, Sept., 14~17, 1997

Lee, S. K. and White, P. R., 1997, "Fault diagnosis of rotating machinery using Wigner Higher Order Moment Spectra," Mechanical Systems and Signal Processing, Vol. 11, No. 4, p. 637 ~650.

Lee, S. K, 1998, "Adaptive Signal processing and Higher Order Time Frequency Analysis and Their Application to Condition Monitoring," Ph. D. thesis, ISVR, The University of Southampton, U. K.

McFadden, P. D., 1987, "Examination of a Technique for the Early Detection of Failure in Gears by Signal Processing of the Time Domain Average of the Meshing Vibration," Mechanical Systems and Signal Processing Vol. 1, pp. 177 ~183.

O'Neill, J. C., 1995, "Quadralinear Time-Frequency Representations," Proceeding of ICASSP, pp. 1005~1008.

Randall, R., 1982, "A New Method of Modelling Gear Faults," ASME, Trans. Journal of Mechanical Design, Vol. 1, pp. 259-267.

Reynolds, A. G., 1995, " The Detection of Local tooth defections in gearing by vibration analysis," MSc. Thesis, Royal Naval Engineering College, Manadon, Plymouth.

Staszewski, W. J. and Tomlinson, G. R., 1994, "Application of the wavelet transform to fault detection in a spur gear," Mechanical System and Signal Processing Vol. 8, 289~307.

Staszewski, W. J. and Tomlinson, G. R., 1997, "Local Tooth Fault Defection in Gear Boxes Using a Moving Window Procedure," Mechanical System and Signal Processing, Vol. 11, pp. 331 ~350.

Stankovič, L., 1994, "A Multitime Definition of Wigner Higher Order Distribution : L-Wigner Distribution," IEEE Signal Processing Letter, Vol. 1, pp. 106~225.

Stankovič, L., 1996, "Auto-term Representation by the Reduced Interference Distribution : A Procedure for Kernel Design," IEEE Transaction on Signal Processing, Vol. 44, pp. 1557~1563.

Stankovič, L., 1996, "L-Class of Time- Frequency Distributions," IEEE Signal Processing Letters, Vol. 3, pp. 22~25.

Wang, W. J. and McFadden, P. D., 1995, "Decomposition of gear Motion Signals and Its Application to Gearbox Diagnostics," ASME Trans. Journal of vibration and Acoustics, Vol. 117, p. 363~369.

Wang, W. J. and McFadden, P. D., 1996, "Application of Wavelet to Gearbox Vibration Signals for Fault Detection," Journal of Sound and Vibration, Vol. 192, pp. 927~939.